ΔT_m = logarithm temperature difference, °F.
λ = latent heat at saturation temperature, B.t.u./lb.
μ_i = water viscosity at bulk water temperature, lb./(ft.)(hr.)
μ = viscosity of condensate evaluated at film temperature, lb./(ft.)(hr.)
μ_w = water viscosity at average inside wall temperature, lb./(ft.)(hr.)
ρ = density of condensate evaluated at film temperature, lb./cu. ft.

LITERATURE CITED

1. Nusselt, W., *Z. Ver. Deut. Ing.*, **60**, 541, 569 (1916).
2. Jakob, M., "Heat Transmission," Vol. 1, Wiley, New York (1949).
3. Katz, D. L., E. H. Young, and G. Balekjian, *Petrol. Ref.*, **33**, No. 11, 175-178 (1954).
4. Katz, D. L., and J. M. Geist, *Trans. Am. Soc. Mech. Engrs.*, **70**, No. 11, 907-914 (1948).
5. Short, B. E., and H. E. Brown, in "Proceedings of the General Discussion on Heat Transfer," Sect. I, pp. 27-31, Am. Soc. Mech. Engrs. and Inst. Mech. Engrs. (London) (1951).
6. Young, F. L., and W. J. Wohlenberg, *Trans. Am. Soc. Mech. Engrs.*, **64**, No. 11, 787-794 (1942).
7. Watson, R. G. H., J. J. Brunt, and D. G. P. Birt, in "International Developments in Heat Transfer," Pt. II, Am. Soc. Mech. Engrs., New York (1961).
8. Othmer, D. F., *Ind. Eng. Chem.*, 21, 576 (1929).
9. Hampson, H., in "Proceedings of the General Discussion on Heat Transfer," Am. Soc. Mech. Engrs. and Inst. Mech. Engrs. (London) (1951).
10. Briggs, D. E., and E. H. Young, *Rept. No. 55, 01592-149-T*, Office Res. Admin., Univ. Michigan, Ann Arbor (December, 1963).

Manuscript received September 30, 1964; revision received June 18, 1965; paper accepted July 23, 1965. Paper presented at A.I.Ch.E. Boston meeting.

Flow and Turbulence in a Stirred Tank

LOUIS A. CUTTER

Columbia University, New York, New York

Photographic measurements have been made of the mean and fluctuating components of velocity of water in a fully baffled stirred tank. Confirmation of much of the photographic data was obtained with a Kiel impact tube. Eulerian correlation coefficients and also Eulerian scales of turbulence were calculated from the photographic data. The Eulerian scale was of the same order as the blade dimensions, a result consistent with earlier measurements on the turbulence behind grids.

Equations have been developed to describe the flow of energy and the conservation of angular momentum in the impeller stream of a stirred tank with a radial flow impeller and vertical baffles. These are simplifications of the Navier-Stokes equations and the energy equation. They relate energy, angular momentum, and pressure to the mean and fluctuating components of velocity in the impeller stream.

The equations derived are used with the photographic data on mean and fluctuating velocities to estimate the angular momentum at different radial sections of the tank and to calculate the flow of energy through these sections. The estimates are compared with more accurate values of the total torque and energy determined with a torque table.

The objective of the work presented here is the description of the flow of a Newtonian fluid (water) in a fully baffled stirred tank, with particular emphasis on local rates of energy dissipation.

Concern with local rates of energy dissipation is based on the frequently made observation that power per unit volume (or power per unit mass) is often a very useful criterion of agitation, particularly in processes in which one phase is dispersed in another. Kolmogoroff's (*13*) theory of local isotropy provides an explanation of this observation in terms of the intensity of the small-scale eddies in the turbulent flow, since his theory predicts that these eddies are isotropic and that their intensity in a turbulent flow of sufficiently high Reynolds number is dependent only on the local rate of energy dissipation and the viscosity of the fluid. He also predicts that for turbulence of a sufficiently high Reynolds number (higher than is necessary for the first hypothesis to apply) there will be a subrange of eddies, sufficiently large so that they account for a negligible proportion of the viscous energy dissipation and at the same time sufficiently small so that they satisfy the conditions of the first hypothesis. The intensity of eddies in this intermediate range is a function only of their size and of the local rate of energy dissipation per unit mass, ϵ.

Hinze (*11*) has shown that these hypotheses can be used to correlate data by Clay (5) on the breakup of droplets between a rotating and stationary cylinder.

Calderbank (*4*) and Shinnar (*20*) have applied these ideas to the breakup of liquid droplets in another liquid phase and also to the breakup of gas bubbles in a liquid. Shinnar showed that Vermeulen's (*26*) data on the breakup of liquid droplets and gas bubbles could be correlated in terms of a Weber number characteristic of the turbulent stresses predicted by Kolmogoroff's hypotheses.

If Kolmogoroff's theory is to be used extensively, and particularly if it is to be used for scale-up, it becomes important to obtain information about the distribution of energy dissipation rates in a stirred tank as well as the average value.

Louis A. Cutter is with Koppers Company, Inc., Monroeville, Pennsylvania.

There are several statements in the literature that indicate that the flow is very far from being homogeneous, but there is almost no quantitative data on the subject. Calderbank (*4*), however, found that the size of the drops produced varied to a large degree with position in the tank. Sullivan and Lindsey (*21*) indicated that inhomogeneity of the flow of their tank may have been the reason for their failure to get results in accordance with Kolmogoroff's theory. Metzner and Taylor (*16*) estimated rates of energy dissipation in viscous flow with both Newtonian and non-Newtonian fluids. They measured mean velocity gradients from photographs of the flow and found that the greater part of the energy dissipation occurred in the neighborhood of the impeller.

A few other studies have been made of the flow in stirred tanks. Sachs and Rushton (*19*) and Tennant (*22*) used a photographic technique, measuring the velocities of suspended liquid droplets to measure fluid velocities.

Aiba (*1*), operating at higher Reynolds numbers, measured the mean velocity using the deflection of a suspended steel ball to obtain his velocity distribution for a number of different impellers and calculated energy dissipation rates from the mean velocity gradients. He found that for baffled tanks most of the energy dissipation was through turbulence, except when the clearance between the impeller and the baffles was small. All these observers have found that the mean velocity was proportional to the impeller speed.

Nielsen (*18*) has improved on the technique used by Sachs and Rushton (*19*) for measuring fluid velocities and has made a beginning on measurements of turbulence in a stirred tank. He measured the mean velocity distribution, the discharge capacity, and the rate of entrainment of the stream from a mixer turbine. He also determined the vertical and radial components of the turbulent velocity $\sqrt{\overline{u^2}}$, $\sqrt{\overline{v^2}}$, the shear stress in the liquid due to turbulence $t = \rho\overline{uv}$, and the shear correlation coefficients $R = \dfrac{\overline{uv}}{\sqrt{\overline{u^2}\ \overline{v^2}}}$. He found that $\sqrt{\overline{u^2}}$ and $\sqrt{\overline{v^2}}$ had roughly the same magnitude as the mean velocities.

Manning and Wilhelm (*15*) have measured concentration fluctuations in a stirred tank of the same design and from them have obtained energy spectra and Eulerian microscales of turbulence.

THEORETICAL

All velocities outside the impeller stream are assumed negligible compared with those in the impeller stream. Vertical mean velocities are assumed negligible compared with radial and tangential components. Circular symmetry is assumed in all velocity components, as is symmetry between the top and bottom halves of the impeller stream. It is also assumed that the mixer has reached a steady state so that the mean velocity or the mean square of a fluctuating component is no longer a function of time. This does not mean that there are assumed to be no nonrandom fluctuations in velocity but simply that the time means and variances of velocity at any given point in the tank are independent of time, when estimated from a sufficient number of measurements, taken over a sufficiently long interval of time.

Goldstein (*10*) has presented the Navier-Stokes equations and the equation of continuity in cylindrical polar coordinates, the most convenient system to use for the analysis of the flow in a cylindrical tank. The equation of motion in the vertical direction is as follows:

$$U\frac{\partial U}{\partial x} + V\frac{\partial U}{\partial r} + W\frac{\partial U}{\partial \phi} = -\frac{1}{\rho}\frac{\partial P}{\partial x} - \left[\frac{\partial \overline{u^2}}{\partial x} + \frac{1}{r}\frac{\partial r\,\overline{uv}}{\partial r}\right] + \nu\nabla^2 U \qquad (1)$$

Since circular symmetry is assumed, $\partial/\partial\phi = 0$. To a first approximation, $U = 0$. The viscous forces may be neglected in comparison with the inertia forces, because the impeller is operating under conditions such that the power consumption is independent if the viscosity. Thus (1) reduces to

$$0 = -\frac{1}{\rho}\frac{\partial P}{\partial x} - \left[\frac{\partial \overline{u^2}}{\partial x} + \frac{1}{r}\frac{\partial r\overline{uv}}{\partial r}\right] \qquad (2)$$

The group $\overline{uv}$ is likely to be considerably smaller than $\overline{u^2}$, since $\overline{uv}$ will be zero at the center line of the impeller stream and probably will reach a maximum of about 1/2 $\overline{u^2}$ [see Laufer's (*14*) measurements of $\overline{uv}$ in a pipe]. Furthermore, the variation in mean velocity and in mean square velocity will be much less rapid in the radial direction, in which the mean flow is large, than in the vertical direction, in which it is very small. Roughly

$$\frac{\partial \overline{u^2}}{\partial x} = -\frac{1}{\rho}\frac{\partial P}{\partial x}$$

Then

$$\int_o^x \frac{\partial \overline{u^2}}{\partial x}\,dx = -\frac{1}{\rho}\int_o^\infty \frac{\partial P}{\partial x}\,dx \qquad (3)$$

with the boundary conditions:

$$\overline{u^2} = 0 \qquad x = \infty \qquad P = P_o$$

The equation of motion in the radial direction is

$$U\frac{\partial V}{\partial x} + \frac{1}{r}\frac{\partial rV^2}{\partial r} - \frac{W^2}{r} = -\frac{1}{\rho}\frac{\partial P}{\partial r} - \left(\frac{\partial \overline{uv}}{\partial x} + \frac{1}{r}\frac{\partial r\overline{v^2}}{\partial r} - \frac{\overline{w^2}}{r}\right) + \nu\left(\nabla^2 V - \frac{V}{r^2}\right) \qquad (4)$$

The equation of continuity is

$$\frac{\partial U}{\partial x} + \frac{1}{r}\frac{\partial rV}{\partial r} = 0 \qquad (5)$$

By using the equation of continuity, neglecting the viscous terms and substituting

$$\rho\left(\frac{P_o}{\rho} - u^2\right) = P \text{ for } P \qquad (6)$$

one gets

$$\frac{\partial UV}{\partial x} + \frac{1}{r}\frac{\partial rV^2}{\partial r} - \frac{W^2}{r} = \frac{\partial u^2}{\partial r} - \left(\frac{\partial \overline{uv}}{\partial x} + \frac{1}{r}\frac{\partial r\overline{v^2}}{\partial r} - \frac{\overline{w^2}}{r}\right) \qquad (7)$$

After one substitutes

$$\frac{\partial \overline{u^2}}{\partial r} = \frac{\partial \overline{u^2} r}{r\,\partial r} - \frac{\overline{u^2}}{r} \qquad (8)$$

the equation may be integrated at constant r from $X = 0$ to $X = \infty$. Boundary conditions are

$$V = \overline{uv} = 0 \text{ at } X = 0 \text{ all velocities} = 0 \text{ at } x = \infty.$$

Integrating, one gets

$$\int_0^x \frac{\partial(UV + \overline{uv})}{\partial x}\,dx + \frac{1}{r}\frac{dr}{dr}\int_0^x (V^2 + \overline{v^2} - u^2)\,dx = \int_0^\infty \frac{W^2 + \overline{w^2} - \overline{u^2}}{r}\,dx \quad (9)$$

The first term is zero on account of the boundary conditions. The equation can then be reduced to the following:

$$\int_0^x (V^2 + \overline{v^2} - \overline{u^2})\,dx = \int_0^\infty (W^2 + \overline{w^2} - \overline{u^2})\,dx \quad (10)$$

If the turbulence approaches isotropy, and $\overline{v^2} \approx \overline{w^2} \approx u^2$, this equation may be simplified further:

$$\int_0^\infty V^2\,dx = \int_0^x W^2\,dx \quad (11)$$

The third equation of motion gives perhaps the most immediately useful information:

$$U\frac{\partial W}{\partial x} + V\frac{\partial W}{\partial r} + \frac{VW}{r} = -\frac{\partial \overline{uw}}{\partial x} + \frac{\partial \overline{vw}}{\partial r} + \frac{2\,\overline{vw}}{r} + \nu\left(\nabla^2 W - \frac{W}{r^2}\right) \quad (12)$$

Neglecting the viscous terms, collecting like terms, and using the equation of continuity in the same way as before, one obtains

$$\frac{\partial(WU + \overline{wu})}{\partial x} + \frac{\partial r^2(WV + \overline{wv})}{r^2\,\partial r} = 0 \quad (13)$$

When one integrates from $x = 0$ to $x = \infty$ with the same assumptions as before

$$\int_0^x \frac{\partial(WU + \overline{wu})}{\partial x}\,dx + \partial r^2 \frac{\int_0^\infty (WV + \overline{wv})}{r^2\,\partial r}\,dx = 0 \quad (14)$$

Then

$$r^2\int_0^\infty (WV + \overline{vw})\,dx = \text{const.} \quad (15)$$

These equations are an expression for the conservation of angular momentum. This relationship is extremely useful and will be applied later.

Another relationship important to the understanding of the flow in the tank is the energy equation, obtained by multiplying each of the Navier-Stokes equations by its own velocity and adding them [see Laufer (*14*) and Townsend (*23*)]. When one neglects the terms for the viscous diffusion of energy, the equation may be presented as follows:

$$\frac{\partial K^2 U}{\partial x} + \frac{\partial K^2 Vr}{r\,\partial r} + \frac{2\partial(V\overline{u^2} + V\overline{uv} + W\overline{uw})}{\partial x} + \frac{2\partial r(V\overline{v^2} + U\overline{uv} + W\overline{uw})}{r\,\partial r} + \frac{\partial \overline{q^2 u}}{\partial x} + \frac{\partial r\overline{q^2 v}}{r\partial r} = -\frac{2}{\rho}\left[\frac{\partial PU}{\partial x} + \frac{\partial rPV}{\partial r} + \frac{\partial \overline{pu}}{\partial x} + \frac{\partial r\overline{pv}}{r\,\partial r}\right] + 2\epsilon \quad (16)$$

Since

$$\frac{P}{\rho} = \frac{P_0}{\rho} - \overline{u^2},$$

then

$$\frac{1}{\rho}\left(\frac{\partial PU}{\partial x} + \frac{\partial rPV}{\partial r}\right) = \frac{P_0}{\rho}\left[\left(\frac{\partial U}{\partial x} + \frac{\partial rV}{r\,\partial r}\right) - \left(\frac{\partial \overline{u^2}U}{\partial x} + \frac{\partial \overline{u^2}Vr}{r\,\partial r}\right)\right].$$

$$2\epsilon = \partial\left[\frac{K^2 U + 2U\overline{u^2} + 2V\overline{uv} + 2W\overline{uw} + \overline{q^2 u} - 2U\overline{u^2} - \rho\,\overline{pu}}{\partial x}\right] + \frac{\partial r}{r\partial r}\left[K^2 V + 2V\overline{v^2} - 2V\overline{u^2} + 2U\overline{uv} + 2W\overline{vw} + \frac{2\overline{pv}}{\rho} + \overline{q^2 v}\right] \quad (16a)$$

Integrating from $x = 0$ to $x = \infty$ (across half the impeller stream), one notes that at $x = 0$ (center line of the impeller stream), $U = \overline{uv} = \overline{uw} = \overline{q^2 u} = \overline{pu} = 0$. At $x = \infty$ all velocities are assumed negligible. The integral of the whole partial derivative with respect to x is 0:

$$2\int_0^x \epsilon dx = \frac{dr}{rdr}\int_0^\infty \left(K^2 V + 2V\overline{v^2} - 2V\overline{u^2} + 2U\overline{uv} + 2W\overline{vw} + \frac{2\overline{pv}}{\rho} + \overline{q^2}V\right)dx \quad (17)$$

Some terms in this expression can be eliminated without serious error because they are small compared with the others. The judgment used in eliminating terms was derived largely from Laufer's (*14*) study of pipe flow, from Townsend (*23*), and from Corrsin and Uberoi (*6*).

The $q^2 v$ terms are neglected because triple velocity correlation coefficients were found by Laufer to range from 0 at the axis of a pipe to −0.1 or −0.2 at some distance from the axis. The term $2U\overline{uv}$ is neglected on the basis that U is small everywhere, and that $\overline{uv}/u'v'$ is zero at the center line of a jet (*14*) and reaches a maximum of about 0.5. The expression $2\overline{pv}$ can be eliminated in much the same way as $\overline{qv^2}$ terms. Although there are no direct measurements of it to use, $\overline{pv}/p'v'$ is something between 0 and 1. p is probably proportional to $\overline{u^2}$. If this is true, the value of $\overline{pv}$ should be of the same order as $\overline{q^2 v}$. With these deletions, the expression reduces to

$$2\int_0^\infty \epsilon dx = \frac{dr}{rdr}\int_0^\infty (K^2 V + 2W\overline{vw} + 2V\overline{v^2} - 2V\overline{u^2})\,dx \quad (18)$$

Since the values of $\overline{v^2}$ and $\overline{u^2}$ are roughly equal, only a small error will be introduced by making the further simplification $2V\overline{v^2} - 2V\overline{u^2} = 0$. With this step one obtains

$$2\int_0^\infty \epsilon dx = \frac{dr}{rdr}\int_0^\infty (K^2 V + 2W\overline{vw})\,dx \quad (19)$$

In order to calculate the total energy flow through a given annular section, integration in the tangential direction is necessary:

$$2\int_0^{2\pi} rd\phi \int_0^\infty \epsilon dx = \frac{dr}{dr}\int_0^{2\pi} d\phi \int_0^x (K^2 V + 2W\overline{vw})\,dx \quad (20)$$

Performing the indicated integration on the assumption of circular symmetry, and assuming symmetry between the upper and lower halves of the impeller stream, one obtains

$$-\frac{dE}{dr} = 2\pi r\int_{-\infty}^\infty \epsilon dx = \frac{dr}{dr}\,2\pi\int_0^\infty (K^2 V + 2W\overline{vw})\,dx \quad (21)$$

This equation will be used subsequently to estimate the energy flow and dissipation at different sections of the impeller stream.

EXPERIMENTAL

A photographic method was chosen for measuring local fluid velocities which could be used to check the foregoing theory and to estimate local rates of energy dissipation.

The method was an adaptation of Nielsen's (*18*) technique and less directly of Sachs and Rushton's (*19*).

Local fluid velocities were measured by photographing lycopodium particles with a short enough exposure so that the particles showed up in the pictures as short streaks. The necessary light was provided by a flash tube firing through a rotating slotted disk. This system provided enough light to get good pictures on Ilford HPS film with an exposure of 1/600 sec.

The tank used was made of methacrylate plastic 11½ in. I.D. and 12 in. high with a cover to prevent the entrainment of air bubbles. It was built inside a square tank filled with water to minimize distortion in the pictures taken through the side. The tank was always filled so that the cover was submerged during operation. The impeller was a standard Mixing Equipment Company turbine 4 in. in diameter with six flat blades. There were four vertical baffles each a tenth of the tank diameter.

The pictures were examined by projecting them onto the under side of a piece of graph paper on a glass-topped table. Two systems of analysis were used, one for the pictures taken through the bottom of the tank and one for the pictures taken through the side. The pictures taken through the bottom were analyzed with a method primarily designed to give values of the correlation coefficients at different distances. Pairs of vertical parallel lines were drawn on the graph paper one, three, five, thirteen, and twenty-five squares apart (each ½-in square representing 1/29 in. in the tank). One pair of horizontal lines was drawn six squares apart. When a picture was projected on the graph paper, the nearest legible streak to each of the intersections on this grid was traced on the graph paper, and its tangential and radial components were subsequently measured by counting squares. Once a complete series of measurements had been made at any point, the mean velocity, the standard deviation (turbulent component), and the correlation coefficients could be calculated.

For the pictures taken through the side of the tank, a different system of analysis was used, mainly because there was a large velocity gradient in the vertical direction which it was important to measure. No attempt was made to measure correlation coefficients from these pictures. Horizontal lines were drawn two squares apart (each square representing 1/29 in.). Streaks were traced and measured in each of the spaces between the lines, as near as possible to each of two vertical lines, one near each end of the picture. In this way, from each set of pictures, vertical traverses were obtained at two different radial positions.

The photographic method was calibrated by photographing an object of roughly the same size as the particles (the point of a needle taped to one of the impeller blades) moving at a known speed. The impeller speed was determined with a stroboscope calibrated with a reed vibrating at the 60-cycle line frequency.

As a check on the mean velocities measured photographically, measurements were made with a 1/16-in. Kiel (*12*) impact tube. Readings were made in the impeller stream at impeller speeds of 200 to 700 rev./min. as a check on the proportionality of the mean velocity to impeller speed. They were taken at various points in the impeller stream. Readings at 700 rev./min. only were obtained at 0.50 and 0.625 in. from the center line.

Measurements of total torque and power were made with a torque table. Measurements covered the speed range 150 to 450 rev./min.

DISCUSSION OF RESULTS

Mean velocities were determined from photographs taken of the impeller stream in the vertical and horizontal planes at three impeller speeds, 200, 400, and 600 rev./min. The results are plotted in Figures 1 and 2 in terms of the ratio of the local velocity to the blade tip velocity.

The velocity distribution of the impeller stream at each of the three speeds falls on a single curve when plotted in this way. This fact confirms the earlier observations that the local mean velocity at all points is proportional to the impeller speed. It will be noted that the radial and tangential velocities are about equal near the impeller, but that the tangential velocity decreases more rapidly than the radial with increasing radial distance.

The greatest amount of information is available about the velocity distribution on the center line of the impeller stream. At 400 rev./min., thirty pictures were taken at each point, and two streaks from each picture were used at each radial position. Since the standard deviation of the velocity approached the mean, the standard deviation of these means is about 13%. Forty streaks were measured for each radial position at 200 and 600 rev./min. The standard deviation of the mean velocity is about 16%. By using the χ^2 distribution, it is possible to estimate the 90% confidence limits of v' and w' at 400 and 600 rev./min. from the number of streaks measured. At 400 rev./min these are −16.5 and +14%, while at 200 and 600 rev./min. they are −20.4 and +17%.

Because of the high vertical velocity gradient, a different system of analysis was used on the pictures taken through the side of the tank. The same number of pictures was taken, but only one streak from each picture was used at each vertical position. The standard deviation for the mean velocity calculated from these pictures is about 22%. The confidence limits of the vertical turbulent com-

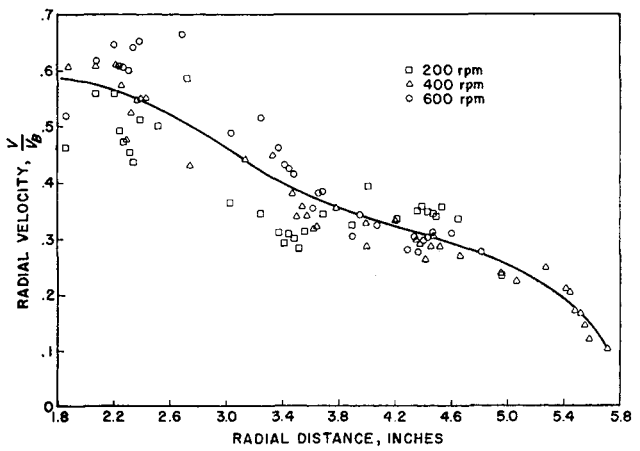

Fig. 1. Radial profile of mean radial velocity on center line of the impeller stream.

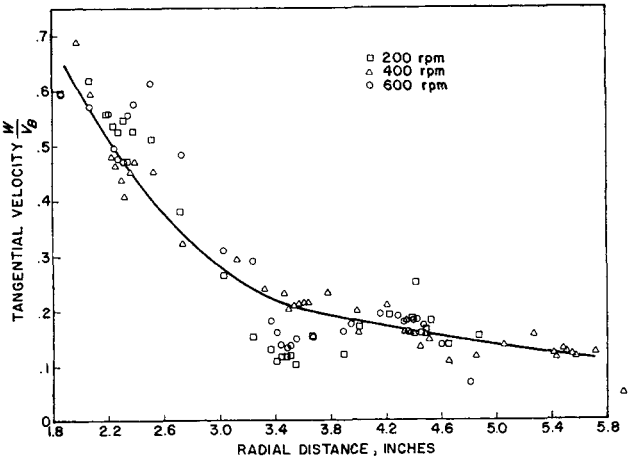

Fig. 2. Radial profile of mean tangential velocity on center line of the impeller stream.

ponent are estimated as −29 and +22% at 200 and 600 rev./min. and −23 and +19% at 400 rev./min.

The Kiel tube measurements give information which makes it possible to check the validity of the mean velocities determined photographically. The impact pressure readings of the Kiel tube are related to velocity as follows:

$$P_i = P - P_o + \frac{\rho}{2g}(U^2 + V^2 + W^2 + \overline{u^2} + \overline{v^2} + \overline{w^2})$$

But $P - P_o \approx -\frac{\rho\overline{u^2}}{g}$. Therefore (22)

$$P_i = \frac{\rho}{2g}(U^2 + V^2 + W^2 - u^2 + v^2 + w^2) \qquad (23)$$

Figure 3 is a plot of $\frac{\sqrt{K^2 - 2\overline{u^2}}}{V_B}$ from the Kiel tube and photographic measurements vs. vertical distance from the center line of the impeller stream near the impeller. Figure 4 is a plot of $\frac{\sqrt{K^2 - 2\overline{u^2}}}{V_B}$ at the center line of the impeller stream vs. radial distance from the axis of the tank. Plotted on the same graphs are values of $\frac{\sqrt{K^2 - 2\overline{u^2}}}{V_B}$ calculated from the photographic measurements. The velocity functions calculated from the two sets of measurements are in reasonable agreement. The flow of the impeller stream at any radial section can be estimated from the quantity

$$\frac{4r}{Dh}\int_o^\infty \frac{\sqrt{K^2 - 2\overline{u^2}}}{V_B}\,dx \qquad (24)$$

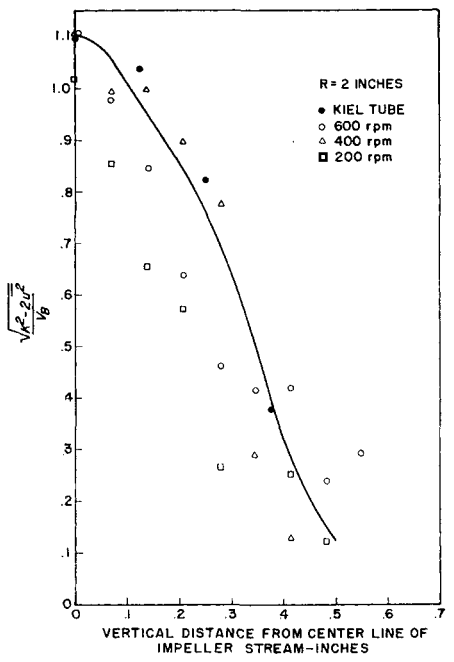

Fig. 3. Vertical profile of resultant velocity (impact tube and photographic) in impeller stream at blade tips.

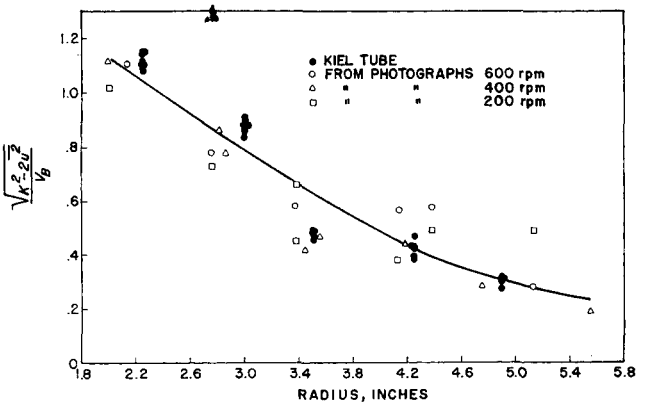

Fig. 4. Radial profile of resultant velocity (impact tube and photographic) in impeller stream.

with Figure 3 and similar curves for other radii used. This expression is the ratio of the flow in the impeller streams at any given radial distance (with circular symmetry assumed) to the flow that would exist at the tips of the impeller blades if the fluid were moving at the blade tip velocity across the sides of the cylinder swept out by the blades. Volume $= \pi\, DhV_B$. The results of this calculation are tabulated below:

R, in.	$\frac{4r}{Dh}\int_o^\infty \frac{\sqrt{K^2 - 2\overline{u^2}}}{V_B}\,dx$	Pumping capacity at 400 rev./min., gal./min.
2.0	0.784	172
2.9	1.04	229
3.5	1.04	229
4.3	1.22	268
4.9	1.07	235

These results are plotted in Figure 5. They show that the formula $V = \pi\, DhV_B$ gives a remarkably close approximation to the total flow in the impeller stream. They are in reasonably good agreement with Sachs and Rushton's (*19*) figures well out in the impeller stream, where $V > W$.

The fluctuating velocity components were estimated from the same pictures as the mean velocity. The ratios

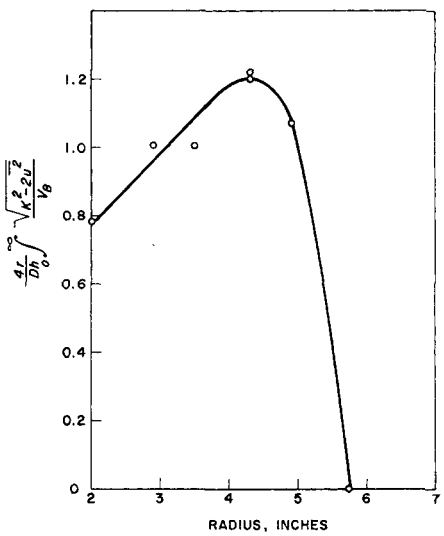

Fig. 5. Radial profile of total flow in impeller stream.

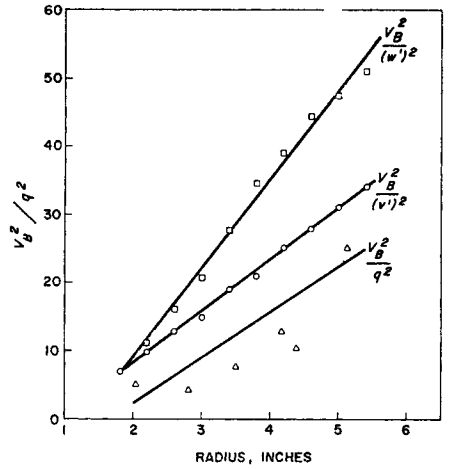

Fig. 6. Decay of turbulence in the radial direction.

of u', v', and w' to V_B also appear to be independent of the impeller speed. Figure 6 presents the ratio V_B^2/v^2, V_B^2/w^2, and V_B^2/q^2 is radial distance. The linear increase in this function, typical of that found by Batchelor (3) in isotropic turbulence and by Townsend (23) in wakes, is also exhibited here. Figure 7 is a typical vertical distribution of the turbulent velocity.

The vertical distribution of the turbulent components appears to be flatter than the mean velocity distribution. For example, near the impeller, at $R = 2$ in., the mean radial velocity drops to half its value at the center line of the impeller stream 0.33 in. away. At the same radius, the standard deviation of the radial velocity drops to half its center-line value in 0.52 in. The vertical spreading of the turbulent velocity distributions with increasing radius roughly follows the spreading of the mean velocity. However, since the turbulent distributions are wider at the start (near the blades), the spreading is proportionally a little less.

In addition to means and standard deviations, correlation coefficients were calculated from the photographs taken in the horizontal plane through the bottom of the tank. Correlation of both radial and tangential velocities was measured at radial distances of 0.0345, 0.104, 0.173, 0.449, and 0.863 in. These measurements were taken over four zones on the center line of the impeller stream and in two zones 1 in. from the bottom of the tank, completely outside the impeller stream. The measurements in the impeller stream were made at 200, 400, and 600 rev./min.

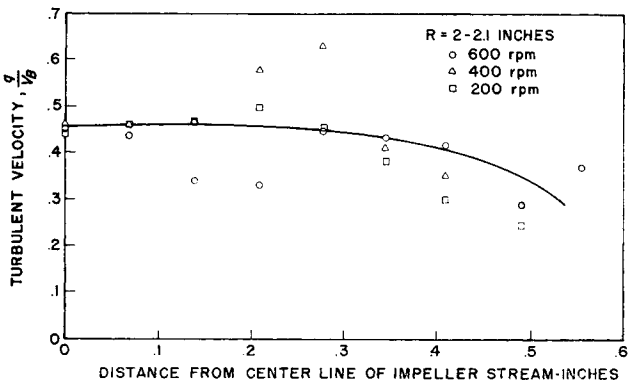

Fig. 7. Vertical turbulent velocity profile at blade tips.

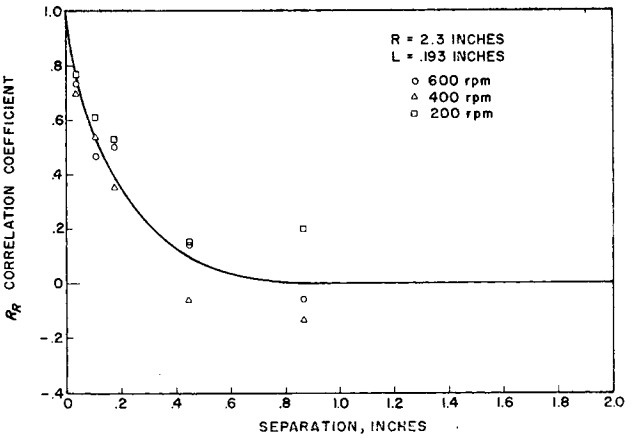

Fig. 8. Radial correlation coefficients at blade tips.

The correlation coefficients and the scales calculated from them are apparently independent of the impeller speed. This observation provides further support for the idea of Reynolds number similarity of the flow at all scales except the scale at which the greater part of the viscous dissipation of energy actually takes place. The data taken at all three speeds were therefore plotted to-

Table 1. Test of von Karman's Equation $g = f + r/2 \dfrac{\partial f}{\partial r}$

r, in.	$\frac{\partial f}{\partial r}$	$\frac{r}{2}\frac{\partial f}{\partial r}$	Correlation coefficients Radial f	Tangential g. cal.	Tangential g. meas.
		$R = 2.3$ in.			
0.0345	−0.25	−0.125	0.74	0.61	0.63
0.104	−0.060	−0.090	0.53	0.44	0.43
0.173	−0.052	−0.130	0.42	0.29	0.30
0.448	−0.024	−0.155	0.11	−0.05	0
0.861	−0.0063	−0.080	−0.02	−0.10	−0.03
		$R = 3.5$ in.			
0.0345	−0.147	−0.074	0.80	0.73	0.74
0.104	−0.054	−0.081	0.68	0.60	0.47
0.173	−0.048	−0.120	0.58	0.46	0.29
0.448	−0.040	−0.260	0.24	−0.02	0.09
0.861	−0.0089	−0.111	0.05	−0.06	0
		$R = 4.4$ in.			
0.0345	−0.144	−0.072	0.80	0.73	0.77
0.104	−0.068	−0.104	0.65	0.55	0.39
0.173	−0.046	−0.114	0.50	0.39	0.25
0.448	−0.0169	−0.110	0.33	0.22	0.09
0.861	−0.0138	−0.173	0.17	0	0
		$R = 5.5$ in.			
0.0345	−0.0452	−0.0226	0.98	0.96	0.74
0.104	−0.119	−0.179	0.70	0.52	0.52
0.173	−0.075	−0.188	0.54	0.35	0.38
0.448	−0.017	−0.110	0.28	0.17	0.03
0.861	−0.009	−0.113	0.11	0	−0.10
		Outside impeller stream 1 in. from bottom			
0.0345	−0.0895	−0.0447	0.92	0.88	0.71
0.104	−0.079	−0.118	0.73	0.61	0.52
0.173	−0.0495	−0.124	0.60	0.48	0.45
0.448	−0.0208	−0.135	0.34	0.20	0.24
0.861	−0.0162	−0.202	0.15	−0.05	0.01

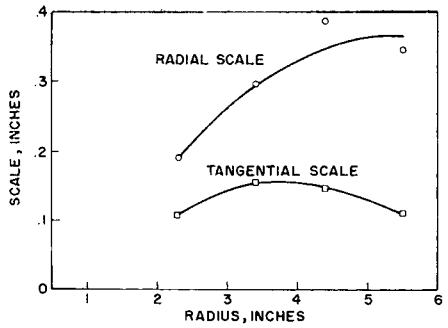

Fig. 9. Scales of turbulence vs. radial distance in the impeller stream.

gether. The correlation coefficients measured in the two zones outside the impeller stream were also plotted together, since the two zones were close together and the flow was not changing rapidly in that region. With these consolidations, it was possible to have a fairly large number of points for each plot of the correlation function. Figure 8 is a typical plot. The correlation coefficient data are summarized in Table 1.

From the correlation plots, scales of turbulence at the center line of the impeller stream have been calculated by graphical integration. They are presented in Figure 9. The values of the scales calculated can be compared with the values determined by Uberoi and Corrsin (25) on air in the region downstream from a screen of a mesh size comparable to the size of the impeller used in the present experiments. The results are remarkably similar in behavior and close in their values, especially when one considers how near the source of turbulence the measurements in the stirred tank were made.

Impeller blades Impeller tip velocity, ft./sec.	1 × 0.8 in. Radial distance from tank axis, in.	Radial scale, in.	Tangential scale, in.
3.5, 7.0, 10.5	2.2	0.193	0.109
	3.5	0.296	0.160
	4.4	0.388	0.149
	5.5	0.346	0.110
Outside impeller stream		0.386	0.243

The radial scale of the stirred tank measurements and the longitudinal scale of Uberoi and Corrsin's measurements (25) have about the same value for comparable sizes of the turbulence generating object. In addition, both seem to increase approximately as the square root of the distance from the source of the turbulence. It might be expected that the radial scale in a stirred tank would be directly proportional to the size of the impeller.

The behavior of the tangential scale is quite different from that of the radial scale, since it reaches a maximum value and then decreases markedly near the wall. The tangential scale at all points is less than the radial scale. Von Karman and Howarth (27) derived the following relationship between correlation coefficients measured in the direction of the flow component f and correlations measured perpendicular to the flow component g, for isotropic turbulence:

correlation coefficient $\quad\quad$ correlation coefficient

$$\overleftarrow{\quad r \quad}\ \rightarrow\ \rightarrow \quad u_1 \quad u_2 \qquad f = \frac{\overline{u_1\, u_2}}{\sqrt{\overline{u_1^2}\ \overline{u_2^2}}} \qquad \overleftarrow{\quad r \quad}\ u_1\uparrow \quad u_2\uparrow \qquad g = \frac{\overline{u_1\, u_2}}{\sqrt{\overline{u_1^2}\ \overline{u_2^2}}}$$

$$g = f + \frac{r}{2}\frac{\partial f}{\partial r} \quad \text{and} \quad L_f = 2\,L_g$$

The radial correlation coefficient is an "f" correlation coefficient, while the tangential is a "g." As a result, if the turbulence approaches isotropy, this relationship might be expected to apply. The values of u', v', and w' are not widely different, and at the axis of the jet the gradients of mean velocity in the vertical direction are zero. The mean velocity gradients in the radial direction remain, however, so that perfect isotropy is not to be expected. Table 1 gives a comparison of values of g calculated from the radial correlation curves compared with values taken from the tangential correlation curves. In the immediate vicinity of the blades, the agreement is very good. At other points the calculated tangential correlation coefficients are higher than the experimental values.

One of the most important calculations carried out with the data on flow in the impeller stream is the estimation of angular momentum at different radial sections. This calculation provides a check on the consistency of the data, since angular momentum should be independent of radial distance between the tip of the impeller and the inner edge of the baffles. These calculations have been carried out for data taken at 200, 400, and 600 rev./min. with the following relationship taken from Equation (15):

$$\frac{Tg_c}{\rho} = = 4\,\pi\, r^2 \int_o^\infty (WV + \overline{wv})\, dx \qquad (15a)$$

The value of the integral across half of the impeller stream was estimated by Simpson's rule. The values of W and w' were available only on the center line of the impeller stream. They were assumed to be in the same proportion to the values of V and v' as at the center line. Values of Tg_c/ρ can be calculated from torque table measurements which are very precise (± 5%) compared with the data on the turbulent flow calculated from the photographs. Figure 10 is a plot of this quantity by both methods plotted against radial distance. They indicate that essentially all of the angular momentum can be accounted for in the impeller stream except in the region close to the wall. Here the flow diverges, and some of the torque is transmitted to the wall by the baffles.

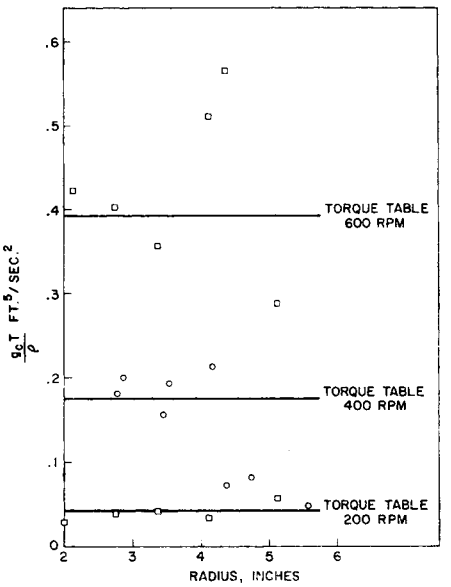

Fig. 10. Comparison of torque table and photographic measurements.

Although the photographic method is capable of a reasonable estimate of the intensity of turbulence, the information gained about the structure of the turbulence is essentially limited to the lower frequency range of the energy spectrum to the eddies containing the bulk of the turbulent energy, not the eddies where the bulk of the dissipation takes place. It is not possible to measure the turbulent velocity gradients directly and gain from them a reliable estimate of the energy dissipation rates. Estimates made in this way were attempted and gave results which were entirely too small to be compatible with the actual power consumption. Indirect methods are therefore necessary. Two were employed. The first is based on the measurement of the rate of disappearance of kinetic energy from the impeller stream.

The total energy passing through any radial section can be estimated in a similar way and compared with the results of the torque table measurements. The equation used was the following one derived in the preceding section:

$$-\frac{dE}{dr} = 2\pi r \int_{-\infty}^{\infty} \epsilon dx = \frac{2\pi dr}{dr} \int_{o}^{\infty} (K^2V + 2W\overline{vw})\, dx \tag{21}$$

The results of the calculation are plotted against radial distance from the axis of the tank in Figure 11. These results show that it is possible to account for approximately 75% of the power in the region next to the impeller and that quite rapid dissipation of the energy takes place in the impeller stream. It is possible to make a rough estimate of the amount of energy which flows out of the impeller stream into the rest of the tank. Examination of Figure 11 indicates that the energy flowing out of the stream is probably between 20 and 40% of the total energy input. For this purpose, the values very close to the wall should be disregarded, because the flow has diverged considerably.

The second method is an empirical one, in which the rate of energy dissipation is estimated from the turbulent velocity and scale of turbulence. These are both properties predominantly controlled by the energy containing eddies, which can be measured readily by the photographic method, rather than of the much smaller energy dissipating eddies.

Batchelor (2) has found that the constant A in the equation is approximately 1.1 for the turbulence behind grids. The reason for using such an equation to estimate the rate of energy dissipation in a stirred tank is that the visible and therefore photographically measurable eddies are the comparatively large ones carrying the bulk of the energy and not the much smaller ones in which the greater part of the energy dissipation takes place. That such an equation can be justified dimensionally can be seen from an examination of the total energy equation given here in Cartesian tensor notation:

$$\frac{U_1\,\partial(\overline{q^2} + U_i^2)}{\partial x_1} + \frac{2\partial U_i\ \overline{u_i u_1}}{\partial x_1} + \frac{\partial \overline{q^2 u_1}}{\partial x_1} =$$

$$-2\frac{\partial(PU_1 + \overline{pu_1})}{\partial x_1} + 2\nu\left[U_i \frac{\partial^2 U_i}{\partial x_1^2} + u_i \frac{\partial^2 u_i}{\partial x_1^2} \right] \tag{25}$$

All the terms except those involving pressures and the viscous terms have the dimensions of velocity^3/length. If the pressure terms are taken as proportional to the square of a velocity, this statement holds for the pressure terms as well. The viscous terms may be broken up as follows:

$$2\nu\left[\frac{\partial^2}{\partial x_j^2} \frac{1}{2} (U_i^2 + \overline{u_i^2}) + \frac{\partial U_i U_j}{\partial x_i x_j} + \frac{\partial \overline{u_i u_j}}{\partial x_i x_j} \right] - \epsilon \tag{26}$$

The first term represents the rate of diffusion of turbulent energy by viscous forces, while the second represents the rate of energy dissipation to heat. Under conditions of very high Reynolds number, the viscous diffusion terms are small compared with the others and can be neglected without much error. The rate of energy dissipation is therefore expressible in terms of a velocity^3/length. The parallel between Batchelor's empirical relationship and the empirical equation for power consumption in a fully baffled stirred tank $\frac{P}{\text{vol.}} \propto \rho N^3 D^2$ is important to notice. The relationship should not be surprising, since both the mean velocity and the fluctuating components appear to be proportional to the impeller speed.

By using the expression $\epsilon = \frac{3}{2}\frac{A(v')^3}{L}$, integrating over the impeller stream, and by assuming the turbulence outside to be homogeneous, one can check whether the earlier calculations of the flow of energy through the impeller stream appear reasonable. These indicated that about 20% of the energy was dissipated in the impeller itself, about 50% was dissipated in the impeller stream, and that the remainder, about 30%, was dissipated in other parts of the tank. The proportions calculated from $\epsilon = \frac{3}{2}\frac{A(v')^3}{L}$ are about the same, 48% in the impeller stream, 16% in the impeller itself, and 36% in the rest of the tank. Total power consumption was calculated as follows:

$$P = \int_{o}^{Vol} \frac{3(v')^3}{2Lg_c}\, \rho dVol \tag{27}$$

Outside the impeller stream the turbulence was assumed to be homogeneous. P', the power input to the impeller stream, is

$$P' = \rho \int_{o}^{R} r \int_{o}^{\infty} \int_{-\infty}^{\infty} 3/2 \frac{(v')^3}{Lg_c}\, dx\, d\phi\, dr \tag{28}$$

The first integration was performed as follows:

$$\int_{-\infty}^{\infty} 3/2 \frac{(v')^3}{Lg_c}\, dx = 3\int_{o}^{\infty} \frac{(v')^3}{Lg_c}\, dx \tag{29}$$

because of vertical symmetry. This integral was evaluated from Simpson's rule at a number of different radial sections from the measurements at all three speeds. The second integration was performed by assuming circular

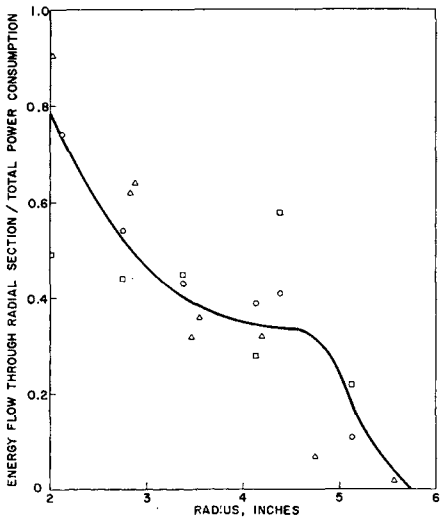

Fig. 11. Radial flow of energy in the impeller stream.

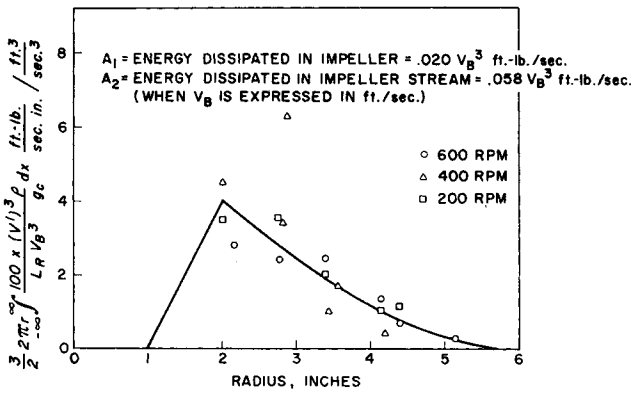

Fig. 12. Energy dissipation vs. radial position in the impeller stream from turbulent velocities.

symmetry at all points in the impeller stream. The final integration was performed graphically from Figure 12. The variable v' was replaced by v'/V_B to reduce the results from different impeller speeds to a single curve. The expression $\frac{4\rho}{gc}\,\pi\, r \int_o^\infty 3/2\, \frac{(v')^3}{LV_B^3}\, dx$ was plotted against radial distance, and the area under the curve multiplied by V_B^3 was used as the estimate of P'. P' includes both the power dissipated in the impeller itself and in the impeller stream. The portion dissipated in the impeller was estimated on the assumption that the energy dissipation was zero at the inner edge of the impeller blades, and it increases linearly across the blade reaching a maximum at the outer edge.

The absolute values of the energy dissipation calculated in this way are not so satisfactory. The average value of A found by Batchelor for fully developed turbulence behind grids was 1.1, while the value required to make the total energy dissipation check with the torque table measurements is 0.34. This discrepancy is much too large to be accidental. There are, however, two well-documented sources for this discrepancy. One is the fact that in the region of the impeller stream, at least, the flow is still developing. Data by Townsend (23, p. 55) indicate that while a flow is developing, the value of A will be less than in more fully developed turbulence. The other source is the fact that intermittency is a characteristic of the turbulence of both wakes and jets (23, pp. 103, 145-146, 190). It is therefore not too surprising if this is also a characteristic of the flow in a stirred tank. In both wakes and jets, there is considerable intermittency of the turbulence over most of the range of mean velocity variation.

Figure 13 is a plot of the ratio $\epsilon/\bar{\epsilon}$ on the center line of the impeller stream. $\epsilon/\bar{\epsilon}$ varies from about 70 near the tips of the blades to about 3.5 near the wall of the tank. Outside the impeller stream $\epsilon/\bar{\epsilon}$ is roughly 0.26. This plot is dramatic evidence that important inhomogeneities in energy dissipation rates can occur in stirred tanks, since a 270-fold difference is observed.

CONCLUSIONS

Mean and fluctuating components of velocity have been measured in a fully baffled stirred tank, with a photographic method used at three different impeller speeds 200, 400, and 600 rev./min. Independent measurements were made of the absolute value of the velocity in the impeller stream with an impact tube. The two methods agreed within the experimental error. Sachs and Rushton (19), and Aiba (1) had observed that this mean velocity was proportional to the impeller speed. Thus, the ratio of local mean velocity to the impeller tip velocity is a function only of position in the tank. These results were confirmed, and it was possible to show that the same statement could be made about u', and v', and w', the root mean square values of the turbulent fluctuations.

Eulerian correlation coefficients and scales were calculated from the pictures taken through the bottom of the tank. The values of the scale agreed quite closely with measurements in a wind tunnel by Uberoi and Corrsin (25) of the scale of turbulence behind grids of the same mesh size as the dimensions of the impeller blades. Furthermore, in both sets of measurements, the scale increased approximately as the square root of distance from the source. The process in the stirred tank, however, occurred over a much shorter distance. Tangential correlation coefficients were calculated from the following equation of von Karman and Howarth (27) valid for isotropic turbulence

$$g = f + \frac{r}{2}\,\frac{\partial f}{\partial r} \qquad (30)$$

and compared with the measured values. Near the impeller blades, the agreement with the isotropic relationship was quite close, but in the vicinity of the wall, the tangential correlations and scale were less than predicted, probably because of the generation of turbulence in connection with the breakup of the impeller stream near the wall.

The increase in the scale of turbulence with distance from the source is an indication that the turbulence in the immediate neighborhood of the blades contains a larger fraction of small eddies than the turbulence further away. These eddies decay faster than the turbulence as a whole, so that the structure of the turbulence is not quite self-preserving. Experiments by Tsjui (24) on the decay of turbulence behind screens of different mesh sizes confirm these ideas. He showed that if two grids, one large and one small, were set up in series, a mixture of large and small scale turbulence would be generated and the small scale turbulence would decay more rapidly than the large scale turbulence.

Using the photographic data on the mean flow and on turbulence, one can calculate the torque at different radial sections of the impeller stream using an equation derived from the tangential Navier-Stokes equation. The results

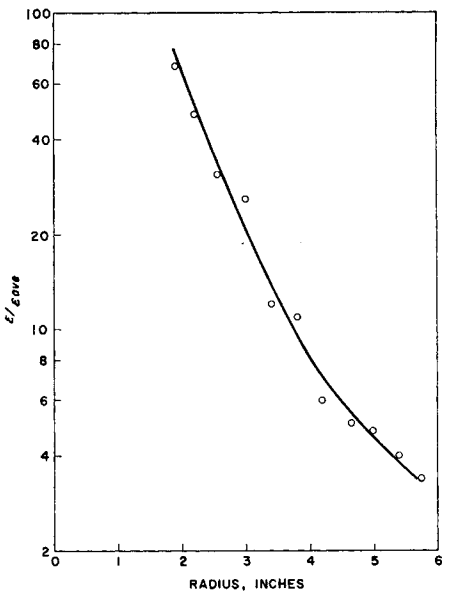

Fig. 13. Comparison of energy dissipation rates on the center line of the impeller stream with the average for the whole tank.

of these calculations were compared with the values from torque table measurements. The results indicated that essentially all of the angular momentum for a tank 12 in. high and 11.5 in. in diameter could be accounted for in the impeller stream which ranges in width from ¾ to 1½ in.

The total flow of energy through different radial sections of the impeller stream was calculated from the photographic measurements, with a modification of the energy equation used. These results were used to estimate the proportions of the energy supplied to the agitator shaft which were being dissipated in the impeller itself, in the impeller stream, and in the rest of the tank. In accordance with this estimate, about 20% of the energy is dissipated in the impeller, about 50% in the impeller stream, and about 30% in the rest of the tank. Confirmation of this estimate was found in the fact that the estimate of energy dissipation from the scale and intensity of turbulence, with the expression $\epsilon = (A_3^{3/2})/(2L)$ used, gave roughly the same proportions, although the values were about three times as high. This discrepancy was probably due to the closeness of the impeller stream to the source of the turbulence and to intermittency of the turbulence. (Good values of the total rate of energy dissipation were available from torque table measurements.)

The flow in a stirred tank with a flat bladed, fully baffled agitator is far from homogeneous. A very large fraction of the flow energy at all frequencies is to be found in the impeller stream, which varies in width in the experimental tank from about h near the blades to about $2h$ near the wall. Most of the energy supplied to the impeller is apparently dissipated in the impeller and the impeller stream, only about 30% being dissipated in the rest of the tank. The value of ϵ/ϵ avg. varies tremendously in this design of stirred tank from 0.25 outside the impeller stream to 70 in the immediate neighborhood of the impeller.

ACKNOWLEDGMENT

The author would like to thank Dr. Sheldon K. Friedlander for his help on the theoretical part of this paper and for introducing him to the fascinating study of turbulence.

The complete data on which this paper is based are presented in a doctoral dissertation by L. A. Cutter (7) available from University Microfilms, Ann Arbor, Michigan. Data have been deposited also as document 8652 with the American Documentation Institute, Photoduplication Service, Library of Congress, Washington 25, D. C., and may be obtained for $7.50 for photoprints or $2.75 for 35 mm. microfilm.

NOTATION

A = constant of proportionality in expression $\epsilon = A\frac{3}{2}\frac{(v')^3}{L}$
D = impeller diameter
E = kinetic energy content of impeller stream of any radial section
f = correlation coefficient measured parallel to flow component
g = correlation coefficient measured perpendicular to flow component
g_c = conversion factor 32, $(lb._m/lb._f)(ft./sec.^2)$
h = impeller width
K^2 = $q^2 + U^2 + V^2 + W^2$
L = Eulerian scale of turbulence $\int_o^\infty R dx$
L_f = scale calculated from f
L_g = scale calculated from g
N = impeller speed, rev./min.
P = total power consumption
P' = power input to impeller stream
P = mean pressure
P_i = impact pressure
P_o = pressure outside impeller stream
p = fluctuating component of pressure
q^2 = $u^2 + v^2 + w^2$
r = radial distance from center line of tank
r' = distance over which correlation is measured
R = Eulerian correlation coefficient, $R = \frac{\overline{u_1 u_2}}{\sqrt{\overline{u_1^2}\ \overline{u_2^2}}}$, u_1 and u_2 are values of fluctuating components of velocity at two points a given distance x apart
T = torque
U, V, W = steady components of velocity
U = vertical
V = radial
W = tangential
Vol = volume
u, v, w = fluctuating components of velocity
u', v', w' = root-mean-square values of fluctuating components
V_n = blade tip velocity
x = vertical distance from center line of impeller stream

Greek Letters

ϵ = energy dissipation per unit mass
μ = viscosity
ν = kinematic viscosity
ρ = fluid density
ϕ = angle specifying tangential position in tank

LITERATURE CITED

1. Aiba, Suichi, Ph.D. thesis, Univ. Tokyo, Japan (1954).
2. Batchelor, G. K., "The Theory of Homogeneous Turbulence," Cambridge Univ. Press, England (1953).
3. ———, *Proc. Cambridge Phil. Soc.*, **43**, 533 (1947).
4. Calderbank, P. H., *Trans. Inst. Chem. Engrs.*, **36**, 443 (1958).
5. Clay, P. H., *Proc. Roy. Acad. Sci. (Amsterdam)*, **43**, 852, 979 (1940).
6. Corrsin, Stanley, and M. S. Uberoi, *Natl. Advisory Comm. Aeronaut. Rept. 998* (1950).
7. Cutter, L. A., D. Eng. thesis, Columbia Univ., New York (1960).
8. Fage, Arthur, *Proc. Roy. Soc.*, **A155**, 577 (1936).
9. Goldstein, Sidney, *ibid.*, 570.
10. ———, "Modern Developments in Fluid Dynamics," pp. 191-233, Oxford Univ. Press, England (1938).
11. Hinze, J. O., *A.I.Ch.E. J.*, **1**, 289 (1955).
12. Kiel, G., *Natl. Advisory Comm. Aeronaut. Tech. Memo 775* (1935); translated from *Luftfahrtforschung*, **12**, 75 (1935).
13. Kolmogoroff, A. N., *Comp. Rend. Acad. Sci. URSS (Doklady)*, **30**, 4 (1941).
14. Laufer, John, *Natl. Advisory Comm. Aeronaut Rept. 1174* (1954).
15. Manning, F. S., and R. H. Wilhelm, *A.I.Ch.E. J.*, **9**, 12 (1963).
16. Metzner, A. B., and J. S. Taylor, *ibid.*, **6**, 109 (1960).
17. Miller, D. R., and E. W. Comings, *J. Fluid Mech.*, **3**, 1 (1957).
18. Nielsen, H. J., Ph.D. thesis, Illinois Inst. Technol., Chicago (1958).
19. Sachs, J. P., and J. H. Rushton, *Chem. Eng. Progr.*, **50**, 597 (1954).
20. Shinnar, Reuel, and J. M. Church, *Ind. Eng. Chem.*, **52**, 253 (1960).
21. Sullivan, D. M., and E. E. Lindsey, *Ind. Eng. Chem. Fundamentals*, **1**, 87 (1962).

22. Tennant, B. W., M.S. thesis, Illinois Inst. Technol., Chicago (1952).
23. Townsend, A. A., "The Structure of Turbulent Shear Flow," Cambridge Univ. Press, England (1956).
24. Tsuji, Hiroshi, *J. Phys. Soc. Japan*, **10**, 579 (1955).
25. Uberoi, M. S., and S. Corrsin, *Natl. Advisory Comm. Aeronaut Rept. 1142* (1953).
26. Vermeulen, Theodore, G. M. Williams, and G. E. Langlois, *Chem. Eng. Progr.*, **51**, 85F (1955).
27. von Karman, Theodore, and Leslie Howarth, *Proc. Roy. Soc.*, **A164**, 192 (1938).

Manuscript received November 25, 1964; revision received August 16, 1965; paper accepted August 19, 1965.

A Two-Way Capillary Viscometer

L. S. TZENTIS

Dow Chemical Company, Williamsburg, Virginia

A two-way capillary viscometer for measuring shear rates from <0.01 to >1,000,000 sec.$^{-1}$ at pressure drops up to 1,000 lb./sq.in. has been designed. It consists of a capillary tube mounted vertically between two sample reservoirs, of which the lower one is connected to a mercury manometer. The driving force, gas under pressure in a large tank, is connected to the upper reservoir and the manometer, thus allowing the sample to be moved in either direction through the capillary. The special feature of this viscometer is the indirect automatic measurement of bulk velocity of the fluid sample (3 to 20 cc.) in the capillary tube by means of a mercury manometer.

The precision of measurement of the velocity is one part in four hundred and can be maintained over the whole range of shear rates by the appropriate choice of the ratio of the diameter of the capillary and manometer tube.

Energy losses due to capillary heating and kinetic energy are given in terms of ΔP across the capillary. Couette end effect was found to be 0.3 diam.

A study of the rheology of polyacrylonitrile (PAN) in concentration range of ½ to 10½% PAN shows that the non-Newtonian behavior and elasticity of PAN solution increases rapidly with concentration.

Because of their simplicity, ease of operation, and construction, capillary viscometers have been popular since the days of Hagen and Poiseuille. Detailed information on the types and methods of correlating data for capillary viscometers is readily available (*1, 2*).

In a capillary viscometer a steady state cannot be established instantaneously. The establishment in the capillary of the final velocity profile of a flowing fluid which is prerequisite for a steady state is delayed by several factors. All occur near or at the contraction made by the capillary joining the reservoir. They are viscous friction at the contraction; the change in kinetic energy of the moving stream entering the capillary; in the isothermal case, the establishment of equilibrium between heat released by friction and heat lost by conduction through the tube walls; and for a viscoelastic fluid, dissipation of energy required to change the shape of the fluid entering the capillary from the reservoir. Corrections for the above factors have to be applied to the data before the true relationship between shear stress and shear rate of the fluid can be established.

One usually avoids most of these corrections by working with capillaries of high L/D ratio to minimize the part of the capillary necessary for the establishment of final velocity profile and, at low shear stresses, to keep the generation of heat due to friction at a minimum. This is fine as long as use of fluids of high viscosities can be avoided. Unfortunately, this is not the case in many modern industries which use polymer solutions of high viscosities.

The two-way capillary viscometer was designed in 1960 in the James River Division of The Dow Chemical Company to investigate the rheological properties of polymer solutions of high viscosities over several decades of shear stress. As the name implies, the two-way capillary viscometer allows one to manipulate the fluid through the capillary in either direction, thus eliminating the need for large samples.

This type of viscometer has been in use since 1950. Westover (*3*) described a capillary rheometer consisting of two rams in opposition at the ends of a capillary with provision for operating at differential pressures up to 25,000 lb./sq. in.

Philippoff (*4*) designed a two-way capillary viscometer with the capillary situated horizontally between two reservoirs. Gas pressure was used to push the fluid alternately between the two reservoirs.

THE TWO-WAY CAPILLARY VISCOMETER

The viscometer, which is immersed in a fluid controlled to within 0.1°C., consists of two stainless steel cylindrical reservoirs (*A*) separated by a capillary (*B*). The reservoirs are screwed into two circular plates (*C*) held together by four screws (see Figure 1). Conical adapters (*D*) at the entrance to the reservoirs minimize entrapment of air bubbles.

The manometer (*E*), used in bulk velocity determination, which in turn is used to calculate the apparent shear rate, is made from a precision glass capillary held together with four aluminum rods (*F*) as shown in Figure 1. The design puts a minimum of strain on the tube, allowing operation at pressures up to 1,000 lb./sq. in. Two photoelectric cells at a fixed distance apart on the manometer tube are used with a mechanical timer and electromechanical clutch to determine flow time to within 0.001 sec. The distance between the photoelectric cells is determined to 0.01 cm. by means of a cathetometer.

METHOD OF OPERATION

The sample is introduced in the lower reservoir (*A*) of the viscometer, which is then assembled and connected to the manometer (*E*) and nitrogen supply (*J*) as shown in Figure